

Phonon dispersion and the competition between pairing and charge order

N.C. Costa,^{1,2,*} T. Blommel,^{2,3} W.-T. Chiu,² G. Batrouni,^{4,5} and R.T. Scalettar²

¹*Instituto de Física, Universidade Federal do Rio de Janeiro Cx.P. 68.528, 21941-972 Rio de Janeiro RJ, Brazil*

²*Department of Physics, University of California, Davis, CA 95616, USA*

³*Department of Physics, North Dakota State University, Fargo, ND 58105, USA*

⁴*Université Côte d'Azur, INPHYNI, CNRS, 0600 Nice, France*

⁵*Beijing Computational Science Research Center, Beijing, 100193, China*

(Dated: December 13, 2017)

The Holstein Model (HM) describes the interaction between fermions and a collection of local (dispersionless) phonon modes. In the dilute limit, the phonon degrees of freedom dress the fermions, giving rise to polaron and bipolaron formation. At higher densities, the phonons mediate collective superconducting (SC) and charge density wave (CDW) phases. Quantum Monte Carlo (QMC) simulations have considered both these limits, but have not yet focused on the physics of more general phonon spectra. Here we report QMC studies of the role of phonon dispersion on SC and CDW order in such models. We quantify the effect of finite phonon bandwidth and curvature on the critical temperature T_{cdw} for CDW order, and also uncover several novel features of diagonal long range order in the phase diagram, including a competition between charge patterns at momenta $\mathbf{q} = (\pi, \pi)$ and $\mathbf{q} = (0, \pi)$ which lends insight into the relationship between Fermi surface nesting and the wavevector at which charge order occurs. We also demonstrate SC order at half-filling in situations where nonzero bandwidth sufficiently suppresses T_{cdw} .

PACS numbers: 71.10.Fd, 71.30.+h, 71.45.Lr, 74.20.-z, 02.70.Uu

Introduction: Quantum Monte Carlo (QMC) methods have evolved into a powerful tool to understand the physics of strongly interacting quantum systems. Nevertheless, many qualitative questions remain largely unaddressed concerning electron-phonon models. One of the most prominent concerns is the origin of charge-density wave (CDW) formation, especially in dimensions greater than one. Increasingly attention has turned to alternatives to the original Peierls picture[1]. Zhu *et al.* have proposed[2, 3] at least three classes of CDWs: (i) those associated with the Peierls instability and Fermi Surface Nesting (FSN), typically in quasi-1D materials; (ii) those driven by a momentum-dependent electron-phonon coupling (EPC), $g_{\mathbf{q}}$, such as the quasi-2D material NbSe₂ [2, 4–9], for which a CDW phase sets in at $T_{\text{cdw}} = 33.5$ K, even though ARPES measurements do not show any sign of FSN[2]; and (iii) systems where electron correlations are implicated in charge modulation, a primary example being the cuprates[10]. In addition to CDW physics, closely related current issues in (high temperature) superconductivity (SC) also invite a return to the study of electron-phonon interactions. For instance, a momentum dependent EPC is believed to be implicated in the dramatic increase in the superconducting transition temperature T_{sc} of FeSe monolayers on SrTiO₂[11–13].

The Random Phase Approximation (RPA) criterion, $4g_{\mathbf{q}}^2/\omega(\mathbf{q}) > 1/\chi_0(\mathbf{q})$, suggests that the shape of the bare phonon dispersion, $\omega(\mathbf{q})$, should affect charge ordering, and hence be important to the analysis of the second class of CDW above. In view of this, here we explore a new scenario in which phonon dispersion plays a primary role in determining the CDW ordering wavevector and critical

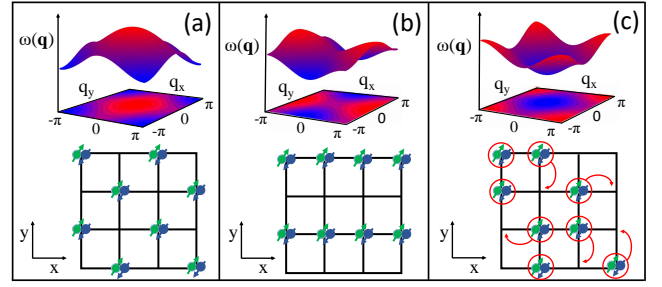


FIG. 1. (Color online) Sketch of bare phonon dispersion (top) and its resulting charge ordering (bottom) for (a) downward curvature, (b) mixed curvature (saddle point at the origin), and (c) upward curvature cases. The arrows on the latter correspond to the (possible) hopping to any available sites and emphasize the possibility of mobile pairs.

temperature, and where SC can supplant diagonal long range order. We extend QMC simulations[14] of a 2D square lattice Holstein Model (HM) to include phonon dispersion[15, 16]. In the HM on a bipartite lattice, CDW order dominates over SC at commensurate filling, similar to the dominance of antiferromagnetism over pairing at half-filling in the Hubbard Hamiltonian[17, 18]. In that model, it is known[19] that off diagonal long range order (ODLRO) can be made more competitive by adjusting the fermionic dispersion relation, e.g. by introducing a next-near-neighbor hopping t' , or via doping. Both these serve to destroy the perfect nesting of the square lattice Fermi surface. Here we adopt a different approach which is available in an electron-phonon model – tuning the phonon dispersion while retaining the features of the bare electronic Fermi surface, i.e. its FSN. The relevance of

such approach can be inferred by its effects on polaron formation, as showed in a recent study, Ref.16. We examine in this Letter the many-electron problem, with our results supporting the picture that the shape of the phonon dispersion plays an important role in the CDW (or SC) formation, i.e. being responsible for enhancing or suppressing it.

Fig.1 presents the qualitative pictures behind our key results: Bare phonon dispersion with (a) downward curvature in going from $\mathbf{q} = (0, 0)$ to $\mathbf{q} = (\pm\pi, \pm\pi)$ leads to an enhancement of the CDW gap and increases T_{cdw} at half-filling; (b) mixed curvature (saddle point at the origin), i.e. upward in \hat{x} and downward in \hat{y} directions, can lead to striped charge order – further emphasizing that charge order and FSN wavevectors do not have to be identical; and (c) upward curvature, which suppresses the CDW gap and, for sufficiently large bandwidth, can initiate a CDW-SC transition at *commensurate filling*.

Methodology: The Holstein model[20],

$$\mathcal{H}_1 = -t \sum_{\langle \mathbf{i}, \mathbf{j} \rangle, \sigma} (d_{\mathbf{i}\sigma}^\dagger d_{\mathbf{j}\sigma} + \text{h.c.}) - \mu \sum_{\mathbf{i}, \sigma} n_{\mathbf{i}, \sigma} + \lambda \sum_{\mathbf{i}, \sigma} n_{\mathbf{i}, \sigma} \hat{X}_{\mathbf{i}} + \frac{1}{2} \sum_{\mathbf{i}} \hat{P}_{\mathbf{i}}^2 + \frac{\omega_1^2}{2} \sum_{\mathbf{i}} \hat{X}_{\mathbf{i}}^2, \quad (1)$$

is one of the simplest tight binding descriptions of the electron-phonon interaction. A single electronic band, with fermionic creation (destruction) operators at site \mathbf{i} , $d_{\mathbf{i}, \sigma}^\dagger$ ($d_{\mathbf{i}, \sigma}$), couples to independent oscillator degrees of freedom $\hat{X}_{\mathbf{i}}$, $\hat{P}_{\mathbf{i}}$. We consider here a square lattice with periodic boundary conditions, nearest neighbor (NN) electron hopping $t = 1$ (to set the scale of energy), chemical potential μ , electron-phonon coupling λ , and local phonon frequency ω_1 .

We generalize Eq. (1) to $\mathcal{H} = \mathcal{H}_1 + \mathcal{H}_2$, to include a ω_2 coupling between NN displacements $\hat{X}_{\mathbf{i}}$, $\hat{X}_{\mathbf{j}}$, with

$$\mathcal{H}_2 = \frac{\omega_2^2}{2} \sum_{\langle \mathbf{i}, \mathbf{j} \rangle} (\hat{X}_{\mathbf{i}} \pm \hat{X}_{\mathbf{j}})^2. \quad (2)$$

We will allow for both signs of this intersite term, i.e. for cases where the sign between neighboring sites $\langle \mathbf{i}, \mathbf{j} \rangle$ in the \hat{x} and \hat{y} directions are equal or different. Physically, the minus sign is the more natural one: forces on atoms depend on their relative displacement. On the other hand, as we discuss below, the positive sign gives a mode with a downward bending momentum 0 to π , the more typical behavior for high frequency optical modes.

The inclusion of NN coupling $\omega_2 \neq 0$ leads to a finite phonon bandwidth $\Delta\omega$. In the absence of the electron-phonon coupling, the quadratic bosonic Hamiltonian can be solved exactly, with bare phonon dispersion relation

$$\omega(\mathbf{q}) = \sqrt{\omega_1^2 + 2\omega_2^2 [2 \pm \cos(q_x) \pm \cos(q_y)]}. \quad (3)$$

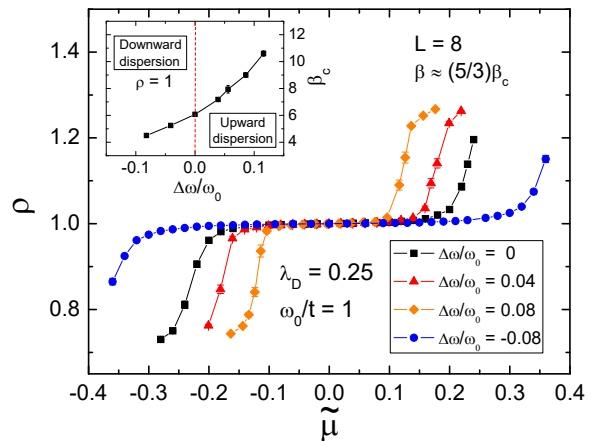


FIG. 2. (Color online) Dependence of electronic density ρ on chemical potential $\tilde{\mu}$, fixing $\lambda_D = 0.25$, $\omega_0/t = 1$ and $\Delta\omega/\omega_0 = 0$ (black squares), 0.04 (red triangles), 0.08 (orange diamonds) and -0.08 (blue circles). The energy scale is fixed for all cases, with $\beta \approx \frac{5}{3}\beta_c$ (i.e. $\beta = 10, 12, 15$ and 8, respectively). Negative and positive signs for the bandwidth $\Delta\omega$ correspond to $\omega(\pi, \pi) < \omega_0$ and $\omega(\pi, \pi) > \omega_0$, respectively. Inset: Inverse critical temperature as a function of $\Delta\omega$. Here, and in all subsequent figures, when not shown, error bars are smaller than symbol size.

Positive signs reduce $\omega(\pi, \pi)$, making it energetically less costly to create a phonon at the M point, while negative signs favor modes at the zone center Γ point, $\omega(0, 0)$ [hereafter ω_0]. A mixed sign breaks rotational symmetry, producing a phonon in the X (or X') point, $\omega(\pi, 0)$ [or $\omega(0, \pi)$]. These three cases, as depicted in Fig.1, are considered in this Letter.

To facilitate discussion of the physics, we introduce dimensionless parameters: (i) the adiabaticity ratio ω_0/t ; (ii) the phonon bandwidth $\Delta\omega/\omega_0$; and (iii) the dimensionless electron-phonon coupling,

$$\lambda_D = \frac{1}{W} \frac{1}{N} \sum_{\mathbf{q}} \frac{\lambda^2}{\omega^2(\mathbf{q})}, \quad (4)$$

which is the polaron binding energy in units of half electronic bandwidth. Here $N = L^2$ is the number of sites, while the electronic bandwidth is $W = 8t$. One can show, through an appropriate particle-hole transformation and shift of the phonon origin, that a half-filled electronic band occurs at $\mu = -\lambda^2/\omega_0^2$, for any dispersion relation $\omega(\mathbf{q})$. We introduce $\tilde{\mu} = \mu + \lambda^2/\omega_0^2$ so that $\rho = 1$ at $\tilde{\mu} = 0$. In what follows, the Hamiltonian parameters λ , ω_1 and ω_2 will be adjusted in order to fix the dimensionless ratios, ω_0/t , $\Delta\omega/\omega_0$ and λ_D .

We examine the features of this generalization of the HM using Determinant Quantum Monte Carlo (DQMC) [21–24]. For details, see the Supplemental Material. The nature of charge ordering is investigated by the equal

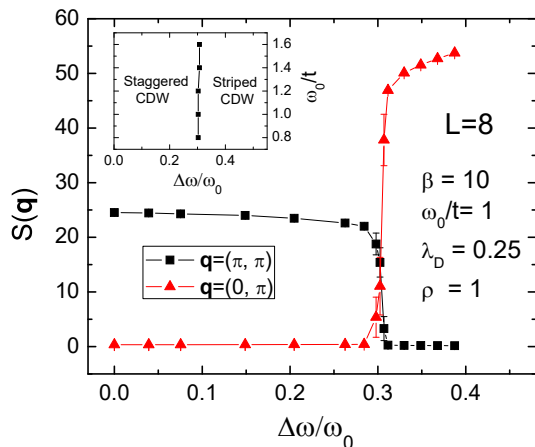


FIG. 3. (Color online) CDW structure factor as a function of phonon bandwidth for the mixed curvature dispersion case, i.e. upward in \hat{x} and downward in \hat{y} directions. A phase transition from staggered to striped order occurs at around $\Delta\omega/\omega_0 = 0.30$, independent of ω_0/t (inset).

time charge-density correlation function,

$$S(\mathbf{q}) = \frac{1}{N} \sum_{\mathbf{i}, \mathbf{j}} e^{i\mathbf{q} \cdot (\mathbf{i} - \mathbf{j})} \langle n_{\mathbf{i}} n_{\mathbf{j}} \rangle, \quad (5)$$

while pairing features are analysed by the s -wave superconducting pair susceptibility

$$P_s = \frac{1}{N} \int_0^\beta d\tau \langle \Delta(\tau) \Delta^\dagger(0) + \text{H.c.} \rangle, \quad (6)$$

with $\Delta(\tau) = \sum_{\mathbf{i}} c_{\mathbf{i}\downarrow}(\tau) c_{\mathbf{i}\uparrow}(\tau)$.

Before presenting our main results on the effects of phonon dispersion on charge and pairing order, we revisit the dispersionless ($\omega_2 = 0$) HM. Quite remarkably, it is only very recently that early simulations[22, 23, 25, 26], for which values of the inverse critical temperature β_c differed by almost 20%, have been followed up to obtain more accurate results for the critical temperature[27, 28]. Fixing $\lambda_D = 0.25$, $\omega_0/t = 1$, at half-filling ($\rho = 1$), we find here that $\beta_c = 6.0 \pm 0.1$. (See Supplemental Material.) This value of β_c is somewhat lower than the earliest DQMC results[23, 25], but in agreement with more recent simulations[27, 28], and will be used as a benchmark when analysing the effects of phonon dispersion. The higher accuracy follows from both advances in raw computer speed, but also improved understanding of the nature of the global moves required to reduce autocorrelation times.

Effect of Dispersion on Charge Correlations: We first consider the case where Eq. (2) has the same sign for both spatial coordinate directions. A positive coupling ($\hat{X}_{\mathbf{i}} + \hat{X}_{\mathbf{j}}$) in Eq. (2) corresponds to $\omega(\pi, \pi) < \omega_0$ and is expected to enhance CDW order. On the other hand, a negative coupling leads to $\omega(\pi, \pi) > \omega_0$ and charge

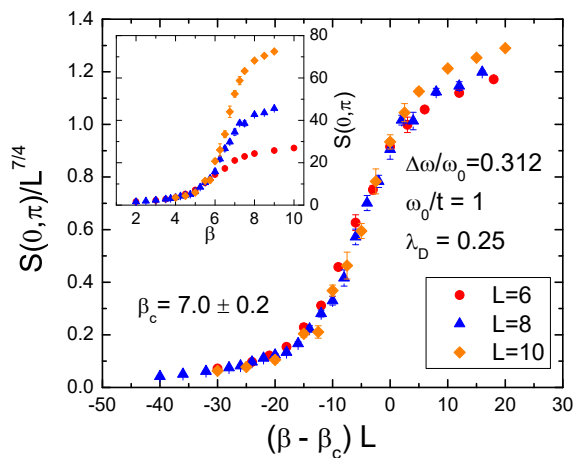


FIG. 4. (Color online) Data collapse of the DQMC results of $S(0, \pi)$ for the mixed curvature (saddle point) case, fixing the 2D Ising critical exponents. Inset: Charge structure factor as function of β . Here $\Delta\omega/\omega_0 = 0.312$.

order at the M point. These two cases correspond to Fig. 1 (a) and (c), respectively. We define $\Delta\omega = \omega(\pi, \pi) - \omega_0$, i.e. $\Delta\omega > 0$ (< 0) for upward (downward) phonon dispersion. The effect of $\omega_2 \neq 0$ is quantified in Fig. 2, which shows the charge gap induced in $\rho(\tilde{\mu})$ by the electron-phonon coupling [29]. This CDW gap grows or shrinks depending on the shape of the phonon dispersion, i.e. if it is downward or upward, respectively. As presented in the inset of Fig. 2, this behavior is accompanied by changes in $\beta_c = 1/T_{\text{cdw}}$, obtained by the same data collapse as used for the dispersionless case. See Supplemental Material. It is remarkable that T_{cdw} can decrease by a factor of two with a relatively small $\Delta\omega/\omega_0 \approx 0.1$.

A mixed sign, in which phonon dispersion terms in Eq. (2) take the form $\hat{X}_{\mathbf{i}} - \hat{X}_{\mathbf{j}}$ for $\mathbf{j} = \mathbf{i} + \hat{x}$ and $\hat{X}_{\mathbf{i}} + \hat{X}_{\mathbf{j}}$ for $\mathbf{j} = \mathbf{i} + \hat{y}$, results in a phonon spectrum with a saddle point at $\mathbf{q} = (0, 0)$, with minima at $\mathbf{q} = (0, \pm\pi)$ and maxima at $\mathbf{q} = (\pm\pi, 0)$, see e.g. Fig. 1 (b). Figure 3 shows the charge structure factors for checkerboard [$\mathbf{q} = (\pi, \pi)$] and striped [$\mathbf{q} = (0, \pi)$], order as a function of the phonon bandwidth $\Delta\omega = \omega(\pi, 0) - \omega(0, \pi)$, for fixed $\lambda_D = 0.25$, $\omega_0/t = 1$, $\beta = 10$ and $L = 8$. In contrast to the case of identical sign, where small $\Delta\omega/\omega_0 \sim 0.1$ had a large effect on the gap and T_{cdw} , the charge correlations here are initially almost independent of $\Delta\omega$ up to $\Delta\omega/\omega_0 \sim 0.25$. However, at $\Delta\omega/\omega_0 \sim 0.30$ a strong suppression of $S(\pi, \pi)$ occurs, with a corresponding rapid rise in $S(0, \pi)$. This transition point is almost independent of ω_0/t , as displayed in Fig. 3 (inset). One should notice that the bare fermion dispersion relation is of course *independent* of $\Delta\omega$, i.e. it retains a nesting at (π, π) and a van-Hove singularity at $\rho = 1$. The onset of striped charge order is initiated by changes in the phonon dispersion, not any alteration to FSN.

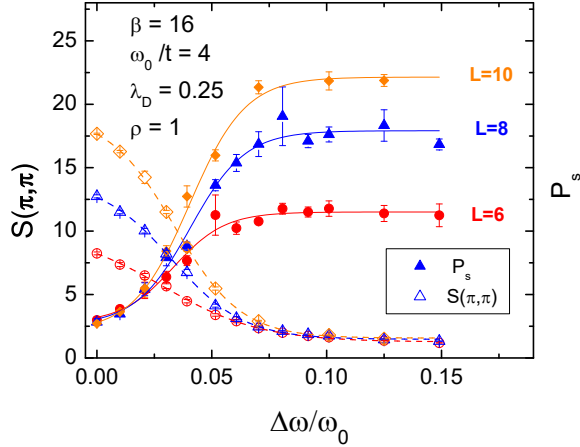


FIG. 5. (Color online) The CDW-SC transition at half-filling: As $\Delta\omega/\omega_0$ increases, $S(\pi,\pi)$ is strongly suppressed while pairing susceptibility P_s is enhanced. Both quantities are in the same scale. Circles, triangles and diamonds correspond to $L = 6, 8$ and 10 , respectively. The filled (open) symbols represent P_s [$S(\pi,\pi)$]. The lines are just guide to the eye.

We can also obtain the transition temperature for the striped phase. The inset of Fig.4 shows raw data for $S(0,\pi)$ on different lattice sizes as a function of β , for $\Delta\omega/\omega_0 = 0.312$, slightly after entry into the striped phase. The corresponding scaling (data collapse) is presented in Fig.4, using the same Ising exponents as for the checkerboard case, Eq.(S3), indicating a finite temperature phase transition at $\beta_c \approx 7.0$.

This striped phase, with $\mathbf{q}_{\text{cdw}} = (0, \pi) \neq 2\mathbf{k}_F$, provides an explicit and quantitative illustration of a non-Peierls CDW instability. Recent experiments have exposed a similar behavior in a variety of materials, i.e. a charge order arising away from $2\mathbf{k}_F$ and whose origin can not be related to the FSN, such as in the quasi-2D materials NbSe₂, CeTe₃, Cr, and U, and also in one dimensional model systems like Au/Ge(001) [2, 7, 30–33]. In particular, NbSe₂ does not exhibit FSN or any divergence in the electronic susceptibility[8], nor a metal-insulator transition. Nevertheless, CDW order sets in at $T_{\text{cdw}} = 33.5\text{K}$. The appearance of this phase, outside the usual Peierls paradigm, is then instead ascribed to strong EPC[2, 3]. As noted earlier, the RPA criterion for CDW order suggests an intimate connection between momentum dependent $g_{\mathbf{q}}$ and phonon dispersion $\omega(\mathbf{q})$, so that the results of Fig. 4 provide a confirmation that additional momentum structure plays a crucial role in the CDW ordering wave vector. We discuss, in the Supplemental Material, possible differences between $g_{\mathbf{q}}$ and $\omega(\mathbf{q})$, which lend some additional complexity.

Effect of Dispersion on Pairing: We now turn to SC order. As noted earlier, it is uncommon for ODLRO to appear in fermionic models at half-filling in bipartite geometries like the square lattice which instead favor

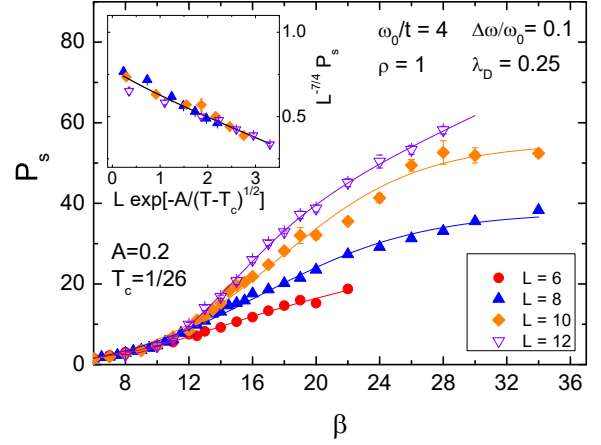


FIG. 6. (Color online) s -wave pair susceptibility as function of the inverse of temperature for $\Delta\omega/\omega_0 = 0.1$, $\omega_0/t = 4$ and $\lambda_D = 0.25$. Inset: the data collapse of the raw DQMC results by Kosterlitz-Thouless scaling for $\beta \geq 16$ (and $L = 8, 10$ and 12). The full lines are just guide to the eye.

diagonal order. Nevertheless, the data of Fig.2 show a rise in β_c with the increased energetic cost for (π,π) CDW formation from the upward phonon dispersion. A natural question is whether that cost eventually becomes prohibitive, opening the door to SC.

To address this, we increase the SC scale of energy and consider phonon frequency $\omega_0/t = 4$. For this case, we obtain $T_{\text{cdw}} \sim 1/13$ for the dispersionless HM ($\omega_2 = 0$), without SC; see Supplemental Material. However, for the dispersive case, $S(\pi,\pi)$ is strongly suppressed at $\Delta\omega/\omega_0 \gtrsim 0.05$, while P_s is enhanced and grows with lattice size, as displayed in Fig. 5, for fixed $\beta = 16$. In words, a CDW-SC transition should occur when $\Delta\omega/\omega_0$ increases. As presented in Fig.6, at $\Delta\omega/\omega_0 = 0.10$, for instance, P_s grows with lattice size for $\beta \gtrsim 12$. In order to establish quasi-long-range order for this case, the appropriate scaling analysis is a Kosterlitz-Thouless (KT) behavior,

$$P_s = L^{2-\eta} f(L/\xi), \quad (7)$$

with $\eta = 1/4$ and

$$\xi \sim \exp\left[\frac{A}{(T - T_c)^{1/2}}\right], \quad T \rightarrow T_c^+. \quad (8)$$

The inset of Fig.6 displays the KT scaling of the P_s raw data for $\beta \geq 16$. Here, the parameters $A = 0.2$ and $T_c = 1/26$ yield the best data collapse. This result provides strong evidence for the onset of SC at half-filling in the HM, when phonon dispersion is taken into account; see also the Supplemental Material. We should mention that recent results[34–39] have also examined the onset of SC in HM, but they have not consider the effects of phonon dispersion.

Conclusions: This paper has provided a significant extension of QMC simulations of electron-phonon Hamiltonians by evaluating the effects of phonon dispersion on charge and pairing order in the Holstein model. The results offer several interesting features, including a CDW-SC transition at half-filling and transitions between CDW phases at different ordering momenta, which are controlled by the bare phonon dispersion. Our findings of non-Peierls CDW phase, despite of existence of FSN on the bare electron dispersion, is of particular interest given recent work calling into question the traditional view of CDW formation [2, 7, 30–33]. In view of this, our results present further insight into the (complex) nature of CDW formation, exhibiting a new avenue to understand and, ultimately, control it.

Acknowledgements: We thank E. da Silva Neto for useful suggestions concerning the manuscript. RTS was supported by Department of Energy grant de-sc0014671, and NCC by the Brazilian agencies Faperj and CNPq. GGB acknowledges support from the University of the Côte d’Azur IDEX Jedi and Beijing CSRC. RTS and GGB acknowledge useful input from K.D. Lewis.

* natanael@if.ufrj.br; natanael.c.costa@gmail.com

- [1] R. Peierls, *Quantum Theory of Solids* (Oxford University, New York, 1955).
- [2] X. Zhu, Y. Cao, J. Zhang, E. Plummer, and J. Guo, *Proceedings of the National Academy of Sciences of the United States of America* **112**, 2367 (2015).
- [3] X. Zhu, J. Guo, J. Zhang, and E. Plummer, *Adv. in Phys. X* **2**, 622 (2017).
- [4] A. Soumyanarayanan, M. Yee, Y. He, J. van Wezel, D. Rahn, K. Rossnagel, E. Hudson, M. Norman, and J. Hoffman, *Proc. Natl. Acad. Sci.* **110**, 1623 (2013).
- [5] C. J. Arguello, S. P. Chockalingam, E. P. Rosenthal, L. Zhao, C. Gutiérrez, J. H. Kang, W. C. Chung, R. M. Fernandes, S. Jia, A. J. Millis, R. J. Cava, and A. N. Pasupathy, *Phys. Rev. B* **89**, 235115 (2014).
- [6] F. Weber, S. Rosenkranz, J.-P. Castellan, R. Osborn, R. Hott, R. Heid, K.-P. Bohnen, T. Egami, A. H. Said, and D. Reznik, *Phys. Rev. Lett.* **107**, 107403 (2011).
- [7] M. D. Johannes and I. I. Mazin, *Phys. Rev. B* **77**, 165135 (2008).
- [8] M. D. Johannes, I. I. Mazin, and C. A. Howells, *Phys. Rev. B* **73**, 205102 (2006).
- [9] M. Calandra, I. I. Mazin, and F. Mauri, *Phys. Rev. B* **80**, 241108 (2009).
- [10] E. Da Silva Neto, P. Aynajian, A. Frano, R. Comin, E. Schierle, E. Weschke, A. Gyenis, J. Wen, J. Schneeloch, Z. Xu, S. Ono, G. Gu, M. Le Tacon, and A. Yazdani, *Science* **343**, 393 (2014).
- [11] Q.-Y. Wang, Z. Li, W.-H. Zhang, Z.-C. Zhang, J.-S. Zhang, W. Li, H. Ding, Y.-B. Ou, P. Deng, K. Chang, J. Wen, C.-L. Song, K. He, J.-F. Jia, S.-H. Ji, Y.-Y. Wang, L.-L. Wang, X. Chen, X.-C. Ma, and Q.-K. Xue, *Chin. Phys. Lett.* **29**, 037402 (2012).
- [12] R. Peng, H. Xu, S. Tan, H. Cao, M. Xia, X. P. Shen, Z. Huang, C. Wen, Q. Song, T. Zhang, B. Xie, X. Gong, and D. Feng, *Nature Commun.* **5**, 5044 (2014).
- [13] Y. Wang, K. Nakatsukasa, L. Rademaker, T. Berlijn, and S. Johnston, *Superconductor Science and Technology* **29**, 054009 (2016).
- [14] S. Li, E. A. Nowadnick, and S. Johnston, *Phys. Rev. B* **92**, 064301 (2015).
- [15] J. L. Raimbault and S. Aubry, *Journal of Physics: Condensed Matter* **7**, 8287 (1995).
- [16] D. J. J. Marchand and M. Berciu, *Phys. Rev. B* **88**, 060301 (2013).
- [17] J. E. Hirsch and S. Tang, *Phys. Rev. Lett.* **62**, 591 (1989).
- [18] S. R. White, D. J. Scalapino, R. L. Sugar, E. Y. Loh, J. E. Gubernatis, and R. T. Scalettar, *Phys. Rev. B* **40**, 506 (1989).
- [19] H. Q. Lin and J. E. Hirsch, *Phys. Rev. B* **35**, 3359 (1987).
- [20] T. Holstein, *Annals of Physics* **8**, 325 (1959).
- [21] R. Blankenbecler, D. J. Scalapino, and R. L. Sugar, *Phys. Rev. D* **24**, 2278 (1981).
- [22] R. T. Scalettar, N. E. Bickers, and D. J. Scalapino, *Phys. Rev. B* **40**, 197 (1989).
- [23] R. M. Noack, D. J. Scalapino, and R. T. Scalettar, *Phys. Rev. Lett.* **66**, 778 (1991).
- [24] R. R. dos Santos, *Brazilian Journal of Physics* **33**, 36 (2003).
- [25] M. Vekić, R. M. Noack, and S. R. White, *Phys. Rev. B* **46**, 271 (1992).
- [26] P. Niyaz, J. E. Gubernatis, R. T. Scalettar, and C. Y. Fong, *Phys. Rev. B* **48**, 16011 (1993).
- [27] N. C. Costa, W. Hu, Z. J. Bai, R. T. Scalettar, and R. R. P. Singh, *Phys. Rev. B* **96**, 195138 (2017).
- [28] M. Weber and M. Hohenadler, arXiv:1709.01096 (2017).
- [29] These results also agree with Max. Entropy Method, as presented in the Supplemental Material.
- [30] M. Maschek, S. Rosenkranz, R. Heid, A. H. Said, P. Giraldo-Gallo, I. R. Fisher, and F. Weber, *Phys. Rev. B* **91**, 235146 (2015).
- [31] D. Lamago, M. Hoesch, M. Krisch, R. Heid, K.-P. Bohnen, P. Böni, and D. Reznik, *Phys. Rev. B* **82**, 195121 (2010).
- [32] S. Raymond, J. Bouchet, G. H. Lander, M. Le Tacon, G. Garbarino, M. Hoesch, J.-P. Rueff, M. Krisch, J. C. Lashley, R. K. Schulze, and R. C. Albers, *Phys. Rev. Lett.* **107**, 136401 (2011).
- [33] C. Blumenstein, J. Schäfer, M. Morresi, S. Mietke, R. Matzdorf, and R. Claessen, *Phys. Rev. Lett.* **107**, 165702 (2011).
- [34] C. Lin, B. Wang, and K. H. Teo, *Phys. Rev. B* **93**, 224501 (2016).
- [35] C. Lin, B. Wang, and K. H. Teo, *Physica C: Superconductivity and its Applications* **532**, 27 (2017).
- [36] C. B. Mendl, E. A. Nowadnick, E. W. Huang, S. Johnston, B. Moritz, and T. P. Devereaux, *Phys. Rev. B* **96**, 205141 (2017).
- [37] I. Esterlis, B. Nosarzewski, E. W. Huang, B. Moritz, T. P. Devereaux, D. J. Scalapino, and S. A. Kivelson, arXiv:1711.01493 (2017).
- [38] T. Ohgoe and M. Imada, *Phys. Rev. Lett.* **119**, 197001 (2017).
- [39] S. Karakuzu, L. F. Tocchio, S. Sorella, and F. Becca, *Phys. Rev. B* **96**, 205145 (2017).
- [40] M. Creutz and B. Freedman, *Annals of Physics* **132**, 427 (1981).

- [41] R. T. Scalettar, R. M. Noack, and R. R. P. Singh, Phys. Rev. B **44**, 10502 (1991).
- [42] M. Jarrell and J. Gubernatis, Physics Reports **269**, 133 (1996).
- [43] G. G. Batrouni, R. T. Scalettar, G. T. Zimanyi, and A. P. Kampf, Phys. Rev. Lett. **74**, 2527 (1995).

Supplemental Material for: Phonon dispersion and the competition between pairing and charge order

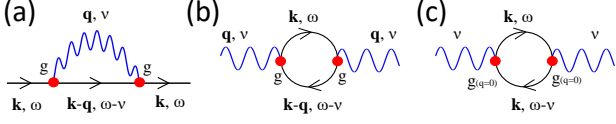


FIG. S1. (Color online) (a) Electron self-energy to second order in perturbation theory, as well as phonon self-energies for (b) phonon dispersion and (c) momentum-dependent electron-phonon coupling cases.

Phonon dispersion and electron-phonon coupling:

Including momentum dependence in the phonon dispersion relation has some qualitative connections to a momentum-dependent electron-phonon coupling, but is rather different when considered in detail. This can be seen, for instance, through a calculation of the lowest-order electron self-energy $\Sigma(k, \omega)$ in Fig. S1 (a),

$$\begin{aligned}\Sigma^g(k, \omega) &\sim \int dq d\nu |g(q)|^2 \frac{1}{\omega - \nu - \epsilon_{k-q}} \frac{2\omega_0}{\nu^2 - \omega_0^2} \\ \Sigma^\omega(k, \omega) &\sim \int dq d\nu |g|^2 \frac{1}{\omega - \nu - \epsilon_{k-q}} \frac{2\omega(q)}{\nu^2 - \omega(q)^2},\end{aligned}\quad (\text{S1})$$

where Σ^g and Σ^ω are the forms for $g(q)$ and $\omega(q)$ respectively. In the $\nu \rightarrow 0$ limit, where the phonon carries no energy, we have that $\Sigma^g = \Sigma^\omega$ under the condition $|g(q)|^2/\omega_0 = |g|^2/\omega(q)$. However it is evident that for nonzero ν the two self-energies are not equal.

Such difference is even more accentuated in the phonon self-energy. For phonon dispersion case, Fig. S1 (b), the phonon self-energy is

$$\Pi^\omega(q, \nu) = \int dk d\omega g^2 \frac{1}{\omega - \epsilon_k} \frac{1}{\omega - \nu_q - \epsilon_{k-q}}, \quad (\text{S2})$$

while for the momentum-dependent electron-phonon coupling case, Fig. S1 (c), one obtains

$$\Pi^g(\nu) = \int dk d\omega |g(q=0)|^2 \frac{1}{\omega - \epsilon_k} \frac{1}{\omega - \nu - \epsilon_k}. \quad (\text{S3})$$

We have written these expressions in conventional real time notation. The expressions appropriate for DQMC are the imaginary-time (Masubara frequency) analogs, but the point, that Σ^g and Σ^ω as well as Π^ω and Π^g are in general inequivalent, is the same. At higher order, e.g. in vertex corrections, the differences between $\omega(q)$ and $g(q)$ approaches will become even more complex.

Determinant Quantum Monte Carlo: We examine the features of the Holstein model (HM) using Determinant Quantum Monte Carlo (DQMC) simulations[21–24]. We first perform the usual mapping[40] of the quantum oscillator degrees of freedom onto a path integral in imaginary time by discretizing the inverse temperature $\beta = \Delta\tau L_\tau$. The degrees of freedom of the fermions

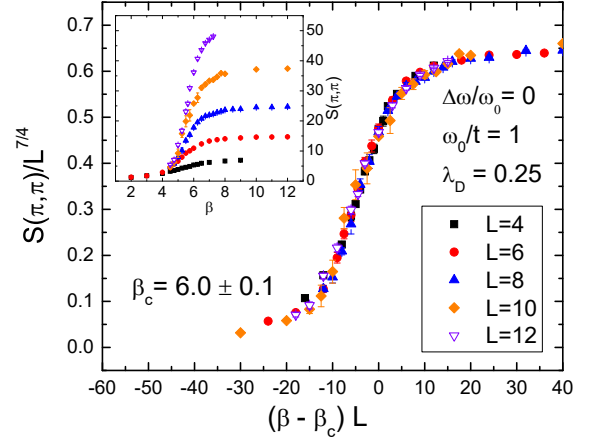


FIG. S2. (Color online) Data collapse of the charge-density correlation function of the dispersionless Holstein model at half filling and fixing $\lambda_D = 0.25$ and $\omega_0/t = 1$ within the 2D Ising universality class. Inset: $S(\pi, \pi)$ as function of inverse of temperature. Here, and in all subsequent figures, when not shown, error bars are smaller than symbol size.

moving in this fluctuating space and imaginary time phonon field can be integrated out analytically, so that the partition function is

$$\begin{aligned}\mathcal{Z} &= \int d\{x_{i,l}\} e^{-\Delta\tau S_B} \left[\det(I + B_1 B_2 \cdots B_L) \right]^2, \\ S_B &= \sum_{\mathbf{i}} \sum_{l=1}^{L_\tau} \left[\frac{1}{2} \left(\frac{x_{\mathbf{i},l} - x_{\mathbf{i},l+1}}{\Delta\tau} \right)^2 + \frac{\omega_1^2}{2} x_{\mathbf{i},l}^2 \right] \\ &\quad + \sum_{\langle \mathbf{i}, \mathbf{j} \rangle} \sum_{l=1}^{L_\tau} \left[\frac{\omega_2^2}{2} (x_{\mathbf{i},l} \pm x_{\mathbf{j},l})^2 \right].\end{aligned}\quad (\text{S4})$$

Here $\int d\{x_{i,l}\}$ is the integral over the (continuous) space- and imaginary time-dependent phonon field. S_B is the bosonic action. The determinant appears as a square because the two fermionic species $\sigma = \uparrow, \downarrow$ experience the same phonon field and contribute identically to \mathcal{Z} . An important consequence is the *absence of a sign problem at any filling*. The matrices B_l are each a product of an exponential of the hopping term in Eq. (1) and an exponential of a site-diagonal matrix containing the phonon variables at that imaginary time slice l .

The physical quantities of interest are obtained by sampling the phonon fields $\{x_{i,l}\}$ and measuring combinations of the equal time fermion Green's function $G = [I + B_1 B_2 \cdots B_{L_\tau}]^{-1}$. We keep $\Delta\tau$ small enough (in most of cases $\Delta\tau = 0.1$) so that Trotter errors are less than the statistical errors from the Monte Carlo sampling. We should stress that, in addition to local moves of single phonon coordinates, we also implemented *global* moves[41], which reduce autocorrelation times. Despite of that, our simulations were performed with a large number of Monte Carlo steps, in most of cases larger

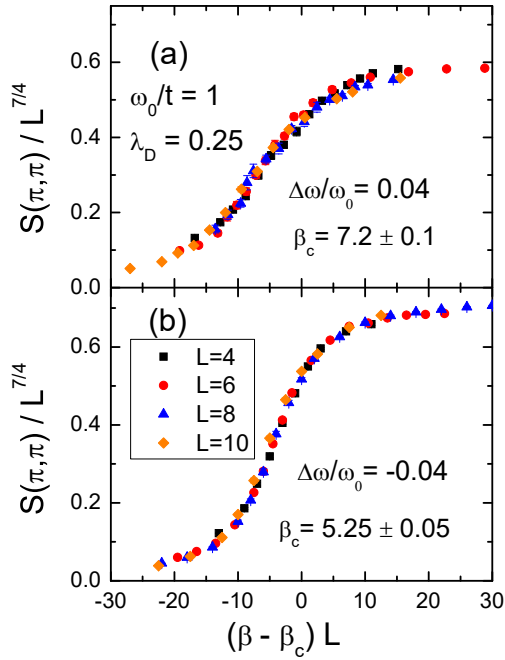


FIG. S3. (Color online) Data collapse of $S(\pi, \pi)$ for different lattice sizes at (a) $\Delta\omega/\omega_0 = 0.04$ and (b) -0.04 , and fixing $\lambda_D = \omega_0/t = 1$.

than 2×10^5 .

Data collapse ($\Delta\omega/\omega_0 = 0$): The inset of Fig. S2 shows the charge-density correlation function for the parameters of Refs. 23 and 25, $\lambda_D = 0.25$ and $\omega_0/t = 1$ and half-filling, $\rho = 1$. $S(\pi, \pi)$ exhibits a strong dependence on spatial lattice size for $\beta \gtrsim 5$. A precise determination of the transition temperature is obtained via finite size scaling. Since the HM exhibits a finite temperature phase transition which breaks \mathbb{Z}_2 (spin-inversion) symmetry, the transition belongs to the two-dimensional Ising universality class, and hence,

$$S(\pi, \pi) = L^{2-\eta} f(L(\beta - \beta_c)^\nu), \quad (\text{S5})$$

with $\eta = 1/4$ and $\nu = 1$. Fixing these exponents, the data collapse is presented in Fig. S2, with $\beta_c = 6.0 \pm 0.1$.

Data collapse ($\Delta\omega/\omega_0 \neq 0$): Regardless the phonon dispersion, i.e. if it is downward or upward, the staggered CDW phase still has a discrete order parameter and breaks the \mathbb{Z}_2 (spin-inversion) symmetry. Thus, the T_{cdw} can be obtained by performing a data collapse of the DQMC data points using the scaling function of Eq. (S5), similarly to the previous case. For instance, Fig. S3 exhibits the data collapse for (a) $\Delta\omega/\omega_0 = 0.04$ [downward case] and (b) $\Delta\omega/\omega_0 = -0.04$ [upward case] at fixed $\lambda_D = 0.25$ and $\omega_0/t = 1$. In the former it is obtained $\beta_c \approx 7.2$, while in the latter it is $\beta_c \approx 5.25$. The same procedure is performed to obtain T_{cdw} for other values of $\Delta\omega/\omega_0$.

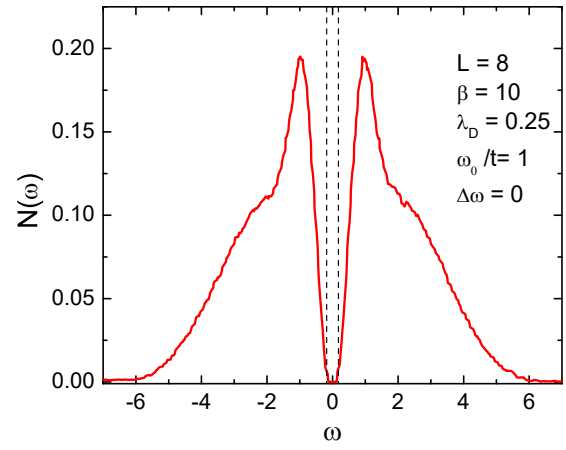


FIG. S4. (Color online) Density of states of the dispersionless Holstein model at $\beta = 8$ and fixed $\lambda_D = 0.25$ and $\omega_0/t = 1$. The vertical dashed lines enclose the charge gap.

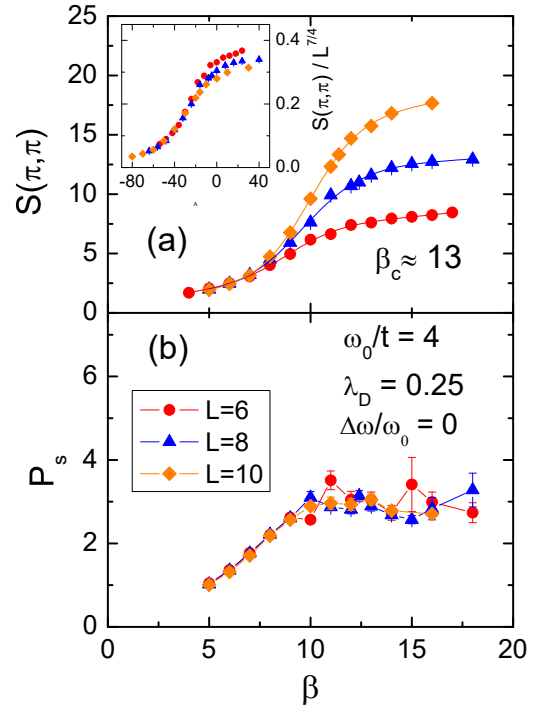


FIG. S5. (Color online) (a) Staggered charge-density structure factor behavior of the dispersionless Holstein model at different lattice sizes and fixed $\omega_0 = 4$ and $\lambda_D = 0.25$. Inset: Its corresponding scaling (data collapse) using Eq. (S5). (b) The s -wave pair susceptibility for the same parameters of panel (a). The solid lines are just guides to the eye.

Density of States: It is also worth examining the spectral properties of the system, namely its density of states (DOS), as an independent check to the results of Fig. 2. To this end, we need to perform an analytic continuation of the imaginary-time dependent Green's function by

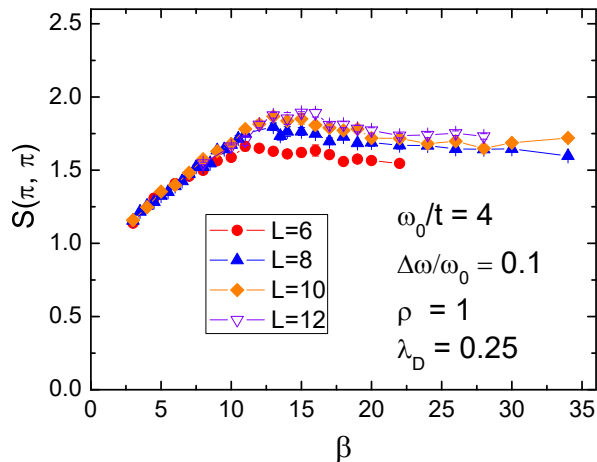


FIG. S6. (Color online) Staggered charge-density structure factor behavior at different lattice sizes for the same parameters of Fig. 6.

inverting the integral equation

$$G(\tau) = \int d\omega N(\omega) \frac{e^{-\omega\tau}}{e^{\beta\omega} + 1}. \quad (\text{S6})$$

This task can be performed by using the Maximum Entropy Method (MEM)[42]. For instance, Fig. S4 exhibits the DOS of the dispersionless Holstein model at

$\beta = 8$ and fixed $\lambda_D = 0.25$ and $\omega_0/t = 1$. The resulting charge gap using MEM is in good agreement with the one presented in Fig. 2.

$S(\pi, \pi)/P_s$ at $\omega_0 = 4$ and $\Delta\omega = 0$: For fixed $\lambda_D = 0.25$ and $\omega_0/t = 4.0$, the $S(\pi, \pi)$ of the dispersionless HM exhibits a strong dependence with lattice size for $\beta \gtrsim 8$, as displayed in Fig. S5(a). Performing the scaling [Eq. (S5)] of this raw DQMC data, as presented in the inset, one finds $\beta_c \approx 13$. This value of $T_{\text{cdw}}(\omega_0 = 4)$ is lower than $T_{\text{cdw}}(\omega_0 = 1)$, even though we have kept $\lambda_D = 0.25$ in both cases. This happens because of the similarities between the Holstein model and the attractive Hubbard model when $\omega_0 \rightarrow \infty$. The latter exhibits a degenerate ground state at half filling, with coexistence between SC and CDW, called a supersolid state[43]. In analogy to spin systems, this corresponds to having both xy (SC) and z (CDW) components of the spin, in which the Mermin-Wagner theorem forbids finite temperature transitions. In view of this, one should expect $T_{\text{cdw}}(\omega_0) \rightarrow 0$ when $\omega_0 \rightarrow \infty$.

On the other hand, the s -wave pair susceptibility exhibits very little dependence with lattice size, as displayed in Fig. S5(b), which supports the picture of a ground state without SC.

P_s at $\omega_0 = 4$ and $\Delta\omega \neq 0$: For completeness we present in Fig. S6 the charge-density structure factor for the same parameters of Fig. 6. This result suggests that CDW is absent at $\Delta\omega/\omega_0 = 0.10$.